# Assignments of Bending Vibrations of Ammonia Adsorbed on Solid Surfaces

| | |
|---|---|
| Journal: | *Catalysis Letters* |
| Manuscript ID: | Draft |
| Manuscript Type: | Original Manuscript |
| Date Submitted by the Author: | n/a |
| Complete List of Authors: | Suganuma, Satoshi; Tottori University, Center for Research on Green Sustainable Chemistry, Graduate School of Engineering<br>Murakami, Yuta; Tottori University, Department of Chemistry and Biotechnology, Graduate School of Engineering<br>Ohyama, Jota; Tottori University, Department of Chemistry and Biotechnology, Graduate School of Engineering<br>Torikai, Tatsuya; MicrotracBEL Corp.,<br>Okumura, Kazu; Kogakuin University, Department of Applied Chemistry, Faculty of Engineering<br>Katada, Naonobu; Tottori University, Department of Chemistry and Biotechnology, Graduate School of Engineering |
| Keywords: | Heterogeneous catalysis < Catalysis, Thermal desorption < Elementary Kinetics, Characterization < Methodology and Phenomena, (FT)IR < Microscopy, Spectroscopy and General Characterisation, Mass Spectrometry < Microscopy, Spectroscopy and General Characterisation, Acid catalysis < Processes and Reactions, DFT < Theory |
| | |

# Assignments of Bending Vibrations of Ammonia Adsorbed on Solid Surfaces

Satoshi Suganuma*[1], Yuta Murakami[2], Jota Ohyama[2], Tatsuya Torikai[3], Kazu Okumura[4], and Naonobu Katada[2]

[1] Center for Research on Green Sustainable Chemistry, Graduate School of Engineering, Tottori University, 4-101 Koyama-cho Minami, Tottori 680-8552, Japan

[2] Department of Chemistry and Biotechnology, Graduate School of Engineering, Tottori University, 4-101 Koyama-cho Minami, Tottori 680-8552, Japan

[3] MicrotracBEL Corp., 1-1-9 Harada-naka, Toyonaka 561-0807, Japan

[4] Department of Applied Chemistry, Faculty of Engineering, Kogakuin University, 2665-1 Nakano, Hachioji, Tokyo 192-0015, Japan

* E-mail: suganuma@chem.tottori-u.ac.jp



## Abstract

Bending vibrations in the infrared (IR) spectra of ammonia adsorbed on Lewis acidic metal oxides, i.e., $Al_2O_3$, $ZrO_2$ and $TiO_2$, and zeolite were analyzed with an aid of density functional theory (DFT) calculations. The results by DFT methods reveal the wavenumbers of the vibration modes ($\nu_4$ and $\nu_2$) of $NH_4$ bonded to Brønsted acid site and the vibration modes ($\delta_s$ and $\delta_d$) of $NH_3$ species coordinated to a Lewis acidic metal center (M = Al, Zr or Ti). The wavenumbers calculated based on DFT were reasonably in agreement with the experimentally observed values. The estimation of wavenumbers suggests that the $\delta_s$ vibration of $NH_3$ hydrogen-bonded is invisible on a zeolite, because it is hidden by an intense absorption due to skeletal vibration. On the other hand, multiple bands of asymmetric bending modes ($\delta_d$ and $\nu_2$) observed on a zeolite were assigned. A quantification method of Brønsted and Lewis acid sites, and hydrogen-bonded $NH_3$ is provided based on the peak assignments.

## Introduction

Ammonia is a gaseous base compound with a small molecular size and therefore widely utilized as a probe for the characterization of acid sites on solid catalysts and other functional materials. It has been known that, by the adsorption of ammonia, an ammonium cation ($NH_4^+$) is formed on a Brønsted acid site, a coordinated $NH_3$ species is formed on a Lewis acid site (metal center), and a hydrogen-bonded (or interacted via specifically strong physical adsorption) $NH_3$ species is formed on polar species such as Si-OH and $NH_4^+$ which has been adsorbed on a Brønsted acid site on solid surfaces [1,2]. The $NH_3$ molecule hydrogen-bonded to $NH_4^+$ can be expressed as $N_2H_7^+$ as proposed [3]. Hereafter these three species, $NH_4^+$ bonded to Brønsted acid site, $NH_3$ coordinated to Lewis acid site and $NH_3$ hydrogen-bonded, are termed $NH_4B$, $NH_3L$ and $NH_3H$, respectively.

Frequencies or wavenumbers in infrared (IR) spectra of the bending vibrations shown in Figure 1 [4] are the keys to identify the adsorbed species as well as the type of adsorption sites. In a low wavenumber region (1100 - 1500 $cm^{-1}$), $\delta_s$ of $NH_3$ and $\nu_4$ of $NH_4$ can be observed, while $\delta_d$ of $NH_3$ and $\nu_2$ of $NH_4$ should appear in a high wavenumber region (1600 - 1800 $cm^{-1}$). The $\delta_s$ of $NH_3$ and $\nu_4$ of $NH_4$ modes are termed symmetric vibrations, whereas the $\delta_d$ of $NH_3$ and $\nu_2$ of $NH_4$ modes are shown as asymmetric vibrations in this paper based on their nature, although the former vibrations are not properly symmetric in some structure.

Niwa et al. developed a method of ammonia IRMS (infrared-mass spectroscopic)-TPD (temperature-programmed desorption) for measurements of the number, strength (enthalpy or energy of ammonia desorption) and type (Brønsted or Lewis) of acid sites on solids [5]. The identification of Brønsted and Lewis acid site is carried out based on the bending frequencies. Practical analysis of the IR spectrum of adsorbed ammonia on a solid sometimes however faces unclear assignments of the bands. Figure 2 shows an example of the temperature dependence of IR spectrum of ammonia adsorbed on a zeolite. Two bands, presumably assigned to symmetric

vibrations ($\delta_s$ of $NH_3$ and $\nu_4$ of $NH_4$), are observed at 1324 and 1444 $cm^{-1}$. The latter should be ascribed to the $\nu_4$ mode of $NH_4B$. The former is assigned to any of $NH_3L$ or $NH_3H$, but further information has not been available. In addition, three bands are found at1627, 1675 and 1760 $cm^{-1}$. The assignments have not been established. It is naturally speculated that the three bands are ascribed to possible three asymmetric modes, i.e., $\nu_2$ of $NH_4B$, and $\delta_d$ of $NH_3L$ and $NH_3H$. It is difficult to answer to the question why the symmetric ($\delta_s$ and $\nu_4$) vibrations reveal the presence of two species while the asymmetric ($\delta_d$ and $\nu_2$) vibrations suggest the presence of three species. On the other hand, the intensities of these bands are decreased with elevating the temperature. The band at 1675 $cm^{-1}$ was almost completely diminished at a relatively low temperature compared to the other asymmetric bands, suggesting the relation of this band to hydrogen bond with a relatively weak interaction. However, the corresponding symmetric band diminishing at a low temperature is not observed in the spectrum.

The aim of this study is to give answers to these questions and to establish the assignments of these vibration bands in order to make possible to quantify each of adsorbed species of ammonia. Theoretical study has been attempted to interpret the vibrations of adsorbed ammonia species in zeolite micropores [3,6]. Density functional theory (DFT) [7] is utilized to estimate the vibration frequencies of related species over Lewis acidic metal oxides such as $Al_2O_3$ and $ZrO_2$ as well as on the zeolite in this study. The calculated wavenumber values are compared to the experimentally observed wavenumbers in order to assign the experimentally observed vibrations. It should be noted that the assignment of symmetric vibration of $NH_4$ bonded to Brønsted acid site, i.e., most important species to interpret the Brønsted acidity, has been established and analyzed theoretically [3,6]. The discussion is focused on the unsolved problems as above.

## Method

### *1. Experimental*

The employed metal oxides, and USY (ultrastable Y) and MOR (mordenite) zeolites are shown in Table 1. The preparation of $TiO_2$ was according to Cao et al. [8], while the USY zeolite was prepared as described in our previous paper [9].

Ammonia IRMS-TPD analysis was carried out using an automatic IRMS-TPD analyzer (MicrotracBEL, Japan). The measurement conditions referred to our previous paper, in which homemade IRMS-TPD analyzer was used [10]. About 7 mg of the sample was compressed into a self-supporting disk with 1 cm of the diameter under 20 MPa, and pre-treated in an oxygen flow (37 μmol $s^{-1}$, 100 kPa) at 823 K for 1 h in an in-situ IR cell. IR spectra were recorded before and after $NH_3$ adsorption. The sample was heated at a ramp rate of 2 K $min^{-1}$ during the elevation temperature from 373 to 823 K in a helium flow (89 μmol $s^{-1}$, 6.0 kPa), and an IR spectrum was collected before and after ammonia adsorption at an interval of 2 K. The concentration of ammonia in the gas phase was monitored by a mass spectrometer (MS) operating at *m/e* 16.

IR spectra at a constant temperature with varying the coverage were obtained using FT/IR-4200 (JASCO, Japan). The sample was pretreated at 823 K in oxygen for 1 h, and then evacuated at 823 K for 1 h. An IR spectrum for the background was measured at 673 K under vacuum. Ammonia was gradually introduced at 673 K. The spectra were collected before the vessel was evacuated and after each evacuation time.

***2. Theoretical***

Model clusters containing $NH_3$ species shown in Table were assumed. Species $NH_3 \rightarrow M$ (M = Al, Zr and Ti) were the employed for modeling $NH_3L$ in entries 1-3. Entry 4, namely, $NH_3$ molecule interacting with an H atom in a silanol group, was adopted for modeling $NH_3H$.

The structural optimization, calculation of total binding energy and analysis of vibrations were carried out using $Dmol^3$ software (Accelrys Inc.) [11] on a generalized gradient approximation (GGA) level using Becke-Lee-Yang-Parr (BLYP) exchange and correlation functional [12]. All electrons were taken into account as well as the relativistic effect. The calculations were performed

using a double numerical polarization (DNP) basis set. The convergence criteria (energy, force and displacement) were set to $2\times10^{-5}$ Ha, $4\times10^{-3}$ Ha Å$^{-1}$ and $5\times10^{-3}$ Å, respectively (1 Ha = $4.360\times10^{-18}$ J = 2625 kJ mol$^{-1}$, 1 Å = $10^{-10}$ m).

## Results

### *1. Experimental*

Figure 3 shows the IR spectra of three metal oxides employed. The contribution of adsorbed ammonia is shown here by a difference spectrum [(spectrum after the adsorption) - (spectrum before the adsorption)]. Bands attributable to the bending vibrations ($\delta_s$ and $\delta_d$) of $NH_3L$ were observed at 1168 and 1599 cm$^{-1}$, respectively, on $TiO_2$. The wavenumbers of both bands on $ZrO_2$, 1173 and 1602 cm$^{-1}$ for $\delta_s$ and $\delta_d$, respectively, were higher than those of the corresponding modes on $TiO_2$. The wavenumber of $\delta_s$ band was further high on $Al_2O_3$ (1224 cm$^{-1}$), and in addition to the $NH_3L$, the band assignable to $\nu_4$ of $NH_4B$ was found at 1466 cm$^{-1}$. Pure γ-$Al_2O_3$ is generally believed to have Lewis acidity only, but the presence of weak Brønsted acid sites which could protonate ammonia was reported [13]. We have reported a similar spectrum of ammonia adsorbed on a different sample of γ-$Al_2O_3$ (a reference catalyst JRC-ALO4) [14]. The asymmetric band on $Al_2O_3$ seems to be separated into two components, 1624 and 1691 cm$^{-1}$. These are speculated to be due to $NH_3$ and $NH_4$. The assignments of these bands will be discussed with an aid of theoretical study in the next section. Before the complete assignments, one can say that any of the wavenumber of $\delta_d$ band on $Al_2O_3$ was higher than those on $ZrO_2$ and $TiO_2$.

Figure 2 shows the IR spectrum of $NH_3$ adsorbed on the USY zeolite. Several bands were observed as stated in the previous section. The large band at 1444 cm$^{-1}$ is presumably ascribed to the $\nu_4$ vibration of $NH_4$ which was formed on the Brønsted acid site. A small band of $\delta_s$ vibration of $NH_3$ was also observed at 1324 cm$^{-1}$. We have to note that the strong absorption around 1200 cm$^{-1}$ by the Si-O skeleton seems to hide the low wavenumber region of this band. In addition, three

bands ascribable to asymmetric vibrations were observed at 1627, 1675 and 1760 $cm^{-1}$.

The temperature dependence of intensities of the five bands on USY was analyzed according to the IRMS-TPD procedure [10]. The absorption spectrum in the range between 1250 and 1850 $cm^{-1}$ was deconvoluted into the fragments as shown in Figure 4. The differentiation of peak area by temperature ($-dA/dT$ where $A$ and $T$ are the absorbance and temperature, respectively), i.e., IR-TPD profile, was calculated to show the desorption rates of ammonia from the corresponding adsorption sites, as shown in Figure 5. The IR-TPD profile of 1675 $cm^{-1}$-band shows that the $NH_3$ desorption had finished at <600 K. The desorption temperature of this 1675 $cm^{-1}$-band was lowest among the IR-TPD profiles of five bands. From the wavenumber (1675 $cm^{-1}$), this peak is assigned to asymmetric vibration of some adsorbed species. However, the corresponding desorption peak due to symmetric vibration in the low wavenumber region was not found at the same temperature. The peak temperature of the IR-TPD of 1627 $cm^{-1}$-band was observed in the next temperature region (420 to 450 K). This peak temperature was similar to that of 1324 $cm^{-1}$-band. The IR-TPD of 1760 $cm^{-1}$-band had the broad peak temperature (450 to 500 K) higher than those of 1627 and 1760 $cm^{-1}$-bands, and similar to that of 1444 $cm^{-1}$-band.

Figure 6 shows difference IR spectra between the spectra measured after pre-treatment and spectra measured after the ammonia adsorption and evacuation on MOR at 673 K. The MOR has strong Brønsted acid sites comparable to USY, and scarcely any Lewis acid sites [9,10]. The large band at 1430 $cm^{-1}$ was assigned to the $\nu_4$ vibration of $NH_4$ which was formed on the Brønsted acid site. The peak position of this band was unchanged even after evacuation for 15 hours. The broad band at 1773 $cm^{-1}$ was ascribed to asymmetric vibrations. The sharp peak at 1625 $cm^{-1}$ attributable to gaseous ammonia disappeared immediately after starting evacuation.

***2. Theoretical***

The structural optimization of assumed clusters was converged into reasonable structures, as the final coordinates are listed in Tables 3 to 8. The wavenumbers calculated are listed in Table .

The optimized structure of $H_3N{\rightarrow}Al(OH)_3$ (entry 1) is shown in Figure 7. The N atom in the $NH_3$ molecule attaches to Al with a distance of 2.062 Å, indicating that this model can represent the nature of $NH_3L$. Both wavenumbers of $\delta_s$ and $\delta_d$ bands gradually shifted higher from entries 1 to 3. It tells us that the frequencies of these bands are dependent on the metal to which $NH_3$ is coordinated as Al > Zr > Ti.

The optimized structure of $H_3N{\cdots}H\text{-}O\text{-}Si(OH)_3$ (entry 4) is shown in Figure 8, indicating that the N atom attaches to H with an N-O distance of 2.840 Å, and therefore hydrogen bond exists between the N and H atoms. It is revealed that the hydrogen-bonded species ($NH_3H$) has 1114 $cm^{-1}$ of $\delta_s$, lower than any of $NH_3$ species coordinated to Lewis acidic metal centers. On the other hand, the wavenumber of $\delta_d$ of this species (1627 $cm^{-1}$) was higher than those of the Lewis acid-coordinated species.

A free $NH_3$ molecule (entry 5) is indicated to have further low $\delta_s$ and high $\delta_d$ wavenumbers. The hydrogen bond, a weaker interaction than the coordination to the Lewis acid center, results in the lower $\delta_s$ and higher $\delta_d$ than those of $NH_3L$ as above. This is in agreement with the observed trend in entry 5 where the lack of atoms surrounding the $NH_3$ molecule provides the low $\delta_s$ and high $\delta_d$ frequencies.

Entries 6-9 show that a $NH_4^+$ cation, formed on a Brønsted acid site, has $\nu_4$ vibrations around 1450 $cm^{-1}$, as observed on a typical Brønsted acidic solid as zeolite, and a $\nu_2$ vibration at the highest wavenumber.

**Discussion**

The $\delta_s$ wavenumbers of $H_3N{\rightarrow}M$ species (M = Ti, Zr or Al) calculated were about 10 to 40 $cm^{-1}$ lower than the wavenumbers experimentally observed in the IR spectra of $NH_3$ adsorbed on the corresponding $MO_x$, which are listed in Table in order to compare these values.

It is reasonable to assign the 1691 and 1624 $cm^{-1}$-bands on $Al_2O_3$ to those of $\nu_2$ of $NH_4$ and

$\delta_d$ of $NH_3$, because the DFT calculations show that the free $NH_4^+$ cation has the highest wavenumber. Subsequently it becomes clear as shown in entries 1-3 (Table ) that the $\delta_d$ wavenumbers of $NH_3L$ calculated were 4 to 20 $cm^{-1}$ higher than the observed values. The shifts of $\delta_s$ and $\delta_d$ bands into high wavenumbers from Ti, Zr to Al in the calculated values were also in agreement with the observations. It seems that the present assumptions of small clusters and the DFT calculations approximately demonstrate the important properties of $NH_3$ species adsorbed on the different metal oxide surfaces.

It is estimated from the DFT calculations that $NH_3H$ had 1114 $cm^{-1}$ of the $\delta_s$ band. Because the calculated values of $NH_3L$ were about 10 to 40 $cm^{-1}$ lower than those of the observed values as above, the actual wavenumber of $NH_3H$ is suspected to be around 1120 - 1150 $cm^{-1}$. It is pointed out that the skeletal vibration of zeolite covers the wavenumber region less than 1250 $cm^{-1}$, and hence the $\delta_s$ vibration of $NH_3H$ at 1120 - 1150 $cm^{-1}$ must be invisible on zeolites. In contrast, the band of $NH_3$ coordinated to Al around 1250 $cm^{-1}$ is believed to be observed, because the high wavenumber region of this band should not be overlapped by the skeletal vibration. The band at 1324 $cm^{-1}$ should be a fraction of the band of $NH_3L$. It is reasonable to use this intense band $\delta_s$ for quantification of the Lewis acid sites, while $NH_3H$ cannot be quantified based on the $\delta_s$ vibration on zeolite.

Multiple bands of $\delta_d$ was observed on $Al_2O_3$ and USY. The DFT indicates that the asymmetric band should appear in the order of wavenumber as $NH_3L < NH_3H < NH_4B$. The three bands found on USY, i.e., the bands at 1627, 1675 and 1760 $cm^{-1}$, are therefore assigned to the $\delta_d$ vibration of $NH_3L$ and $NH_3H$, and the $\nu_2$ mode of $NH_4B$, respectively. The assignment of $NH_3H$ is generally in agreement with the study by Lónyi and Valyon, in which they assigned the IR bands based on the thermal behaviors [15]. The two bands on alumina (1624 and 1691 $cm^{-1}$) can be assigned to $NH_3L$ and $NH_4B$, respectively.

In order to confirm the former assignments, the temperature dependence of the intensities

of three bands on USY was analyzed. The desorption temperature of the species shown by the band at 1675 $cm^{-1}$, assigned to $NH_3H$ as above, was in the lowest starting and end temperature region of desorption. No peak with similar desorption temperature was found in the low wavenumber ($\delta_s$) region. Weak interaction is estimated from the low desorption temperature. These are consistent with the attribution of this band to the $\delta_d$ mode of $NH_3H$, and it is confirmed that the corresponding $\delta_s$ mode was hidden by the skeletal vibration of silicate.

The peak maximum temperature of the IR-TPD of 1760 $cm^{-1}$-band, assigned to $\nu_2$ of $NH_4B$, in the broad temperature region (450 to 500 K), and the temperature range was not significantly different from the peak temperature of IR-TPD of the $\nu_4$ vibration of $NH_4B$ (1444 $cm^{-1}$). This is also consistent with the assignment of 1760 $cm^{-1}$-band to the $\nu_2$ mode of $NH_4B$. In the IR spectra of MOR at the constant temperature, the bands at 1430 and 1773 $cm^{-1}$ was assigned to the $\nu_4$ vibration and the $\nu_2$ mode of $NH_4B$, because it has been clear that MOR has strong Brønsted acid sites. These assignments are consistent with different zeolites.

The IR-TPD of 1627 $cm^{-1}$-band, attributed to $\delta_d$ of $NH_3L$ had the similar peak temperature (420 to 450 K) to that of 1324 $cm^{-1}$-band, assigned to $\delta_s$ of $NH_3L$. This is in agreement with the above discussion in which these bonds were due to the different modes of one species.

The three asymmetric bands at 1627, 1675 and 1760 $cm^{-1}$ on USY have thus been assigned to $NH_3$ coordinated to Lewis acid site, hydrogen-bonded $NH_3$ and $NH_4^+$ bonded to Brønsted acid site. In addition, it is reasonable to quantify the Brønsted acid sites and Lewis acid sites based upon the strong symmetric bands observable at 1444 and 1324 $cm^{-1}$, respectively, while the quantification of hydrogen-bonded species needs analysis of the small $\delta_d$ band at 1675 $cm^{-1}$.

The relationship between MS-TPD, $C_g$ (concentration of ammonia in gas phase), and IR-TPD can be drawn as follows.

$$C_g = \sum \left\{ \frac{\pi D^2 \beta}{4F\varepsilon_i} \left( -\frac{\mathrm{d}A}{\mathrm{d}T} \right)_i \right\} \quad (1)$$

where $D$, $\beta$, $F$, $\varepsilon_i$ and $\left( -\frac{\mathrm{d}A}{\mathrm{d}T} \right)_i$ are the diameter of sample disk, ramp rate, flow rate of carrier gas, molar extinction absorption coefficient of the discussed species and IR-TPD of the discussd species, respectively. The parameter $\varepsilon_i$ is specific to the material and vibration mode, and therefore unknown before experiments. We can estimate through curve-fitting procedure of $C_g$ and $\sum \left\{ \frac{\pi D^2 \beta}{4F\varepsilon_i} \left( -\frac{\mathrm{d}A}{\mathrm{d}T} \right)_i \right\}$ over the temperature range with adjusting the parameters $\varepsilon_i$. The obtained $\frac{\pi D^2 \beta}{4F\varepsilon_i} \left( -\frac{\mathrm{d}A}{\mathrm{d}T} \right)_i$ should be the ammonia TPD spectrum of each kind of adsorption site.

Figure 9 shows the TPD spectra of $NH_4B$, $NH_3L$ and $NH_3H$ derived from the IR-TPD of 1444 $cm^{-1}$-band ($\nu_4$ of $NH_4B$), 1324 $cm^{-1}$-band ($\delta_s$ of $NH_3L$) and 1675 $cm^{-1}$-band ($\delta_d$ of $NH_3H$). It appears that the temperature range of MS-TPD peak was broad, because MS-TPD was the sum of TPD profiles of these three species having different desorption temperature ranges.

The obtained peak area of TPD profile shows the number of each type of adsorption site, whereas the enthalpy or energy of ammonia desorption as an index of adsorption strength can be calculated from the peak area, position and shape [16]. Among them, the numbers and strengths of Brønsted and Lewis acid sites are directly useful for analysis of solid acid catalysis. In contrast, the information from $NH_3H$ should be a noise for the analysis of solid acidic property in most cases. It is believed that separation of the signals due to actual acid sites from the noise is also important. The removal of $NH_3H$ species has been carried out by introduction of water vapor in the conventional technique of ammonia TPD [17-19]. This is owing to the physicochemical nature of ammonia and water; ammonia is a stronger base than water, and therefore ammonia species

adsorbed on an acid site cannot be replaced with water, while an NH bond is less polar than an OH bond, and therefore hydrogen-bonded ammonia is replaced with water. A disadvantage of the water introduction can be raised; nature and microstructure of a surface can be changed by water. The identification of the adsorbed species in the IR spectrum achieved in the present study will extend these techniques to more accurate analysis.

## Conclusions

(1) DFT calculations of the $NH_3$ species coordinated to Lewis acidic metal center gives the reasonable wavenumbers of $\delta_s$ and $\delta_d$ bands.

(2) Bending vibrations of ammonia adsorbed on metal oxides and zeolites are assigned with an aid of DFT. As a result, the wavenumbers of $\delta_s$ and $\delta_d$ vibrations of $NH_3$ hydrogen-bonded are estimated.

(3) On a silicate, it is clarified that the $\delta_s$ vibration of hydrogen-bonded species is invisible because it is hidden by the skeletal vibration, whereas $\delta_d$ of the hydrogen-bonded species can be observed. The other vibrations, i.e., both $\nu_4$ and $\nu_2$ of $NH_4$ bonded to Brønsted acid site and $\delta_s$ and $\delta_d$ of $NH_3$ coordinated to Lewis acid site can be observed.

(4) Quantification of Brønsted and Lewis acid sites, and hydrogen-bonded $NH_3$ is possible by means of an ammonia IRMS-TPD method based on the above peak assignments.

## Acknowledgement

This study was partly supported by a Grant-in-Aid for Scientific Research (B) 23360358 from the Ministry of Education, Culture, Sports, Science and Technology, Japan.

[1] Lónyi F, Valyon J (2001) Thermochim Acta 373:53.

[2] Earl WL, Fritz PO, Gibson AAV, Lunsford JH (1987) J Phys Chem 91:2091.

[3] Zecchina A, Marchese L, Bordiga S, Pazé C, Gianotti E (1997) J Phys Chem B 101:10128.

[4] Nakamoto K, Infrared and Raman Spectra of Inorganic and Coordination Compounds, 6th edition (John Wiley & Sons, New York, 2009).

[5] Niwa M, Katada N, Okumura K, Characterization and Design of Zeolite Catalysts: Solid Acidity, Shape Selectivity and Loading Properties (Springer, Berlin, 2010).

[6] Bučko T, Hafner J, Benco L (2004) J Chem Phys 120:10263.

[7] Sholl DS, Steckel JA, Density Functional Theory: A Practical Introduction (Wiley, Hoboken, 2009).

[8] Cao L, Huang A, Spiess F-J, Suib SL (1999) J Catal 188:48.

[9] Okumura K, Tomiyama T, Morishita N, Sanada T, Kamiguchi K, Katada N, Niwa M (2011) Appl Catal A: Gen 405:8.

[10] Niwa M, Suzuki K, Katada N, Kanougi T, Atoguchi T (2005) J Phys Chem B 109:18749.

[11] Delly B, Ellis DE, Freeman AJ, Baerends EJ, Post D (1983) Phys Rev B 27:2132.

[12] Becke AD (1986) J Chem Phys 104:1040.

[13] Shen Y-F, Suib SL, Deeba M, Koermer GS (1994) J Catal 146:483.

[14] Niwa M, Katada N, Murakami Y (1990) J Phys Chem 94:6441.

[15] Lónyi F, Valyon J (2001) Micropor Mesopor Mater 47:293.

[16] Katada N, Igi H, Kim J-H, Niwa M (1997) J Phys Chem B 101:5969.

[17] Woolery GL, Kuehl GH, Timken HC, Chester AW (1997) Zeolites 19:288.

[18] Bagnasco G (1996) J Catal 159:249.

[19] Igi H, Katada N, Niwa M, Proceedings of the 12th International Zeolite Conference, ed. by Treacy MMJ, Marcus BK, Bisher ME, Higgins JB, Materials Research Society, Warrendale, 1999,

pp. 2643-2650.

Table 1 Employed oxide samples

| Description | Origin |
|---|---|
| $Al_2O_3$ | Reference catalyst JRC-ALO6 supplied by Reference Catalyst Division, Catalysis Society of Japan, as received |
| $ZrO_2$ | Hydrolysis of $Zr(ONO_3)_2$ with $NH_4OH$ in an aqueous solution followed by calcination at 773 K for 4 h |
| $TiO_2$ | Hydrolysis of $Ti[OCH(CH_3)_2]$ with $H_2O$ in ethanol followed by calcination at 773 K for 4 h [8] |
| USY | Small particles (diameter < 50 nm) of USY prepared from a commercial sample of NaY zeolite (HSZ-320NAA from Tosoh, $SiO_2/Al_2O_3$ = 5.5) by ion-exchange with $NH_4NO_3$, steaming at 823 K with $H_2O$ (18 mol%) / $N_2$ and treatment with $NH_4NO_3$ at 353 K [9] |
| MOR | Ion-exchange of JRC-Z-M15 with $Si/Al_2$ = 15 (Reference catalyst, Reference Catalyst Division, Catalysis Society of Japan) with $NH_4NO_3$ at 353 K. |

Table 2 Calculated and observed wavenumbers. All the calculations have been corrected by multiplying with 0.9630, because the OH stretching wavenumber was calculated to be 3798 $cm^{-1}$ under the same conditions while it was observed at 3657 $cm^{-1}$.

| Entry | Description | Wavenumber ($cm^{-1}$) of $\delta_s$ ($NH_3$) or $\nu_4$ ($NH_4$) | | $\delta_d$ ($NH_3$) or $\nu_2$ ($NH_4$) | |
|---|---|---|---|---|---|
| | | calc. | obs. | calc. | obs. |
| 1 | $H_3N{\rightarrow}Al(OH)_3$ | 1206 | 1224[a] | 1602, 1617 | 1624[a] |
| | $H_3N/Al_2O_3$ | 1226 | 1224 | 1593, 1606 | 1624 |
| 2 | $H_3N{\rightarrow}Zr(OH)_4$ | 1134 | 1173[b] | 1566, 1602 | 1602[b] |
| 3 | $H_3N{\rightarrow}Ti(OH)_4$ | 1154 | 1168[c] | 1592, 1630 | 1599[c] |
| | $H_3N/TiO_2$ | 1156 | 1168 | 1613, 1653 | 1599 |
| 4 | $H_3N{\cdots}H\text{-}O\text{-}Si(OH)_3$ | 1123 | | 1601, 1615 | |
| 5 | Free $NH_3$ | 1050 | 1084 | 1607, 1634 | 1627 |
| 6 | $NH_4{\cdots}FAU$ | 1319, 1436, 1495 | 1450[d] | 1640, 1675 | 1674, 1774 |
| 7 | $NH_4{\cdots}BEA$ | 1344, 1472, 1511 | 1450[d] | 1673, 1686 | 1698 |
| 8 | $NH_4{\cdots}MFI$ | 1345, 1473, 1500 | 1450[d] | 1675, 1676 | |
| 9 | $NH_4{\cdots}MOR$ | | 1450[d] | | 1582, 1804 |
| 10 | Free $NH_4^+$ | 1430, 1444, 1473 | | 1681, 1694 | |

a: Observed on $Al_2O_3$. b: Observed on $ZrO_2$. c: Observed on $TiO_2$. d: It looks that a broad band was formed from peaks at 1395, 1445 and 1490 $cm^{-1}$.

Table 3 Final coordinates of entry 1, $H_3N \rightarrow Al(OH)_3$ (Å)

| ID | ATOM | X | Y | Z |
|---|---|---|---|---|
| 1 | N | -4.081580 | 0.773485 | -0.684991 |
| 2 | Al | -2.421710 | -0.000899 | 0.261624 |
| 3 | O | -1.463078 | 1.461537 | 0.385450 |
| 4 | O | -1.945003 | -1.183342 | -0.940260 |
| 5 | O | -3.209663 | -0.585120 | 1.715469 |
| 6 | H | -3.895919 | 1.721776 | -1.025207 |
| 7 | H | -4.871509 | 0.813296 | -0.033480 |
| 8 | H | -4.352062 | 0.192178 | -1.483844 |
| 9 | H | -3.068668 | -1.504843 | 1.985993 |
| 10 | H | -1.036146 | -1.165325 | -1.275970 |
| 11 | H | -1.152732 | 1.738705 | 1.260736 |

Table 4 Final coordinates of entry 2, $H_3N \rightarrow Zr(OH)_4$ (Å)

| ID | ATOM | X | Y | Z |
|---|---|---|---|---|
| 1 | N | -4.168566 | 0.747810 | -1.088112 |
| 2 | Zr | -2.223629 | 0.445466 | 0.507362 |
| 3 | O | -1.337929 | 0.855829 | -1.268799 |
| 4 | O | -2.900826 | -1.442372 | 0.656379 |
| 5 | H | -3.997108 | 1.611308 | -1.610041 |
| 6 | H | -5.080284 | 0.836977 | -0.633345 |
| 7 | H | -4.219785 | -0.011671 | -1.771089 |
| 8 | H | -3.409282 | -1.952950 | 1.302386 |
| 9 | H | -0.375092 | 0.954185 | -1.350894 |
| 10 | O | -0.632334 | 0.427492 | 1.721550 |
| 11 | O | -3.288680 | 1.931244 | 1.395828 |
| 12 | H | -2.968697 | 2.375267 | 2.199095 |
| 13 | H | -0.117290 | -0.222984 | 2.217786 |

Table 5 Final coordinates of entry 3, $H_3N \rightarrow Ti(OH)_4$ (Å)

| ID | ATOM | X | Y | Z |
|---|---|---|---|---|
| 1 | N | -4.092437 | 0.693477 | -1.075752 |
| 2 | Ti | -2.278168 | 0.467780 | 0.460448 |
| 3 | O | -1.374531 | 0.803940 | -1.160820 |
| 4 | O | -2.836046 | -1.306636 | 0.670554 |
| 5 | H | -4.293349 | 1.691254 | -1.178703 |
| 6 | H | -4.956200 | 0.223519 | -0.796682 |
| 7 | H | -3.804529 | 0.330606 | -1.987766 |
| 8 | H | -3.312982 | -1.616478 | 1.459563 |
| 9 | H | -0.413361 | 0.939213 | -1.078482 |
| 10 | O | -0.836793 | 0.534933 | 1.653737 |
| 11 | O | -3.256497 | 1.859914 | 1.266797 |
| 12 | H | -2.848851 | 2.216879 | 2.077195 |
| 13 | H | -0.415759 | -0.282800 | 1.968012 |

Table 6 Final coordinates of entry 4: $H_3N \cdots H_a$-O-$Si(OH)_3$ (Å)

| ID | ATOM | X | Y | Z |
|---|---|---|---|---|
| 1 | N | -3.149728 | 1.931289 | 3.646233 |
| 2 | Si | -2.145739 | -0.054356 | 0.422084 |
| 3 | O | -0.687346 | 0.748297 | 0.516893 |
| 4 | O | -2.609491 | -0.289966 | -1.153493 |
| 5 | O | -1.808672 | -1.499749 | 1.203879 |
| 6 | H | -2.478569 | 2.703158 | 3.620246 |
| 7 | H | -4.046269 | 2.324543 | 3.943574 |
| 8 | H | -2.843868 | 1.294843 | 4.386341 |
| 9 | H | -2.555336 | -2.118869 | 1.261648 |
| 10 | H | -1.916167 | -0.649890 | -1.730019 |
| 11 | H | 0.013948 | 0.231239 | 0.947003 |
| 12 | O | -3.394994 | 0.777003 | 1.062552 |
| 13 | H | -3.281645 | 1.152197 | 1.982249 |

Table 7 Final coordinates of entry 5, free $NH_3$ (Å)

| ID | ATOM | X | Y | Z |
|---|---|---|---|---|
| 1 | N | -0.010477 | -0.014395 | 0.024595 |
| 2 | H | -0.316066 | -0.446786 | -0.852060 |
| 3 | H | -0.315673 | 0.961076 | -0.039395 |
| 4 | H | 1.010932 | 0.022475 | -0.039001 |

Table 8 Final coordinates of entry 6, free $NH_4^+$ (Å)

| ID | ATOM | X | Y | Z |
|---|---|---|---|---|
| 1 | N | -0.034779 | -0.005575 | 0.000586 |
| 2 | H | -0.313716 | -0.461686 | -0.881707 |
| 3 | H | -0.324085 | 0.984404 | -0.017597 |
| 4 | H | 0.989452 | -0.062860 | 0.108671 |
| 5 | H | -0.491362 | -0.481867 | 0.793339 |

**Figure captions**

Figure 1: Vibration modes of $NH_4$ (ammonium cation) and $NH_3$ coordinated to Lewis acidic metal species. ●, ○ and ● show N, H and M (Lewis acidic metal) atoms, respectively.

Figure 2: Difference IR spectra [(spectrum after measured the ammonia adsorption)-(spectrum before measured the ammonia adsorption)] of USY zeolite recorder at every 10 K during temperature elevation.

Figure 3: Difference IR spectra [(spectrum after measured the ammonia adsorption)-(spectrum before measured the ammonia adsorption)] of (A) $Al_2O_3$, (T) $TiO_2$ and (Z) $ZrO_2$.

Figure 4: Deconvolution of IR peaks on USY zeolite at 373 K. $L_s$ and $B_s$ show the assumed bands due to symmetric ($\delta_s$ or $\nu_2$) vibration modes of $NH_3L$ and $NH_4B$, respectively, whereas $L_d$, $H_d$ and $B_d$ show those due to asymmetric ($\delta_d$ or $\nu_4$) modes of $NH_3L$, $NH_3H$ and $NH_4B$, respectively.

Figure 5: IR-TPD spectra (differentiation of peak intensity by temperature) of observed vibration bands on USY. The digits show the wavenumbers of bands. The height of profile is normalized by the maximum value.

Figure 6: Difference IR spectra [(spectrum measured after the ammonia only adsorption or after adsorption and evacuation)-(spectrum measured at 673 K under vacuum after pre-treatment)] of MOR zeolite recorder at each evacuation time.

Figure 7: Optimized structure of Entry 3, $H_3N \rightarrow Al(OH)_3$.

Figure 8: Optimized structure of Entry 4, $H_3N \cdots H\text{-}O\text{-}Si(OH)_3$.

Figure 9: Estimated TPD profiles from corresponding species on USY zeolite. MS shows the profile of ammonia desorption measured by MS.

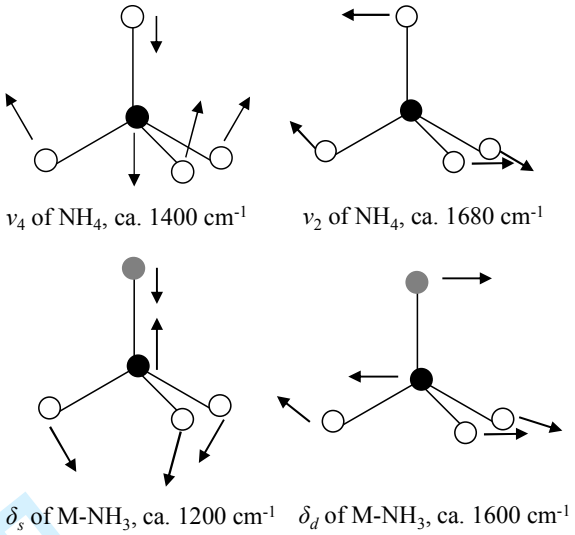


# Figure 1

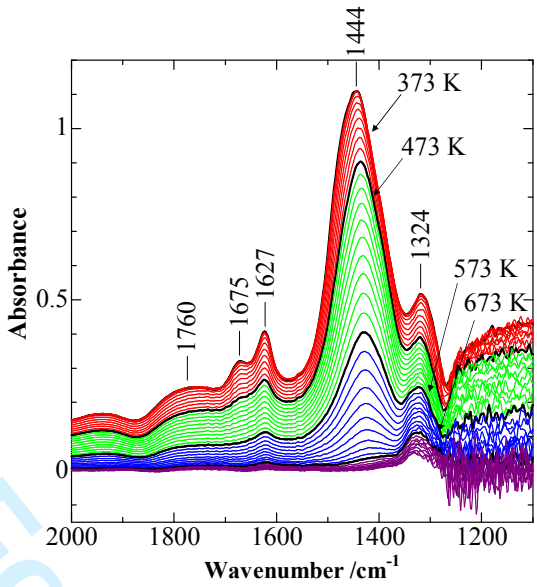


# Figure 2

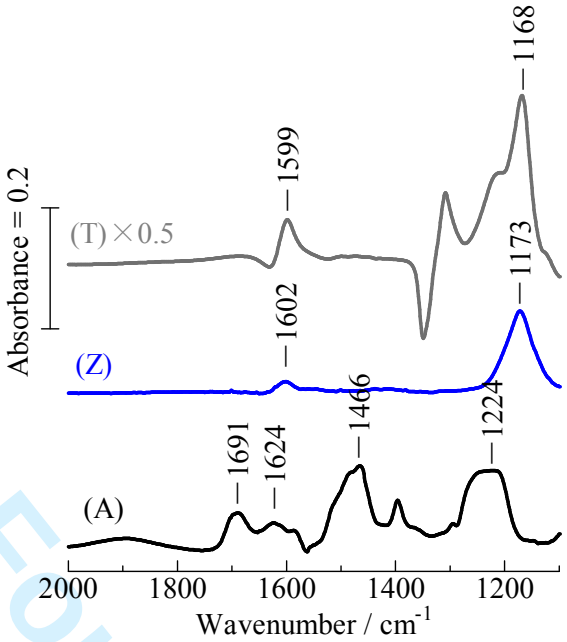


**Figure 3**

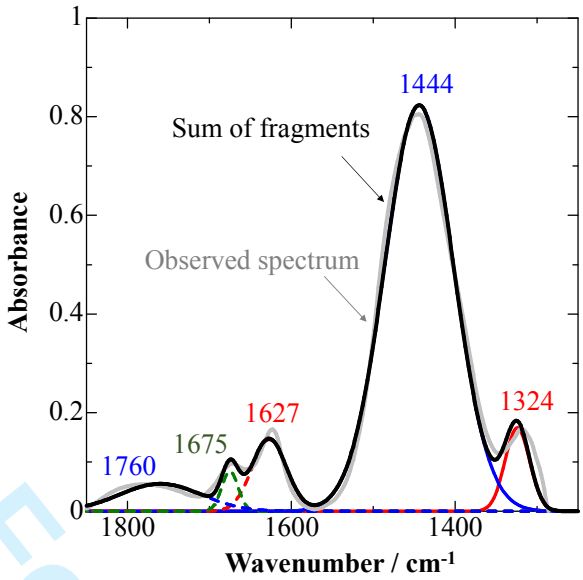


# Figure 4

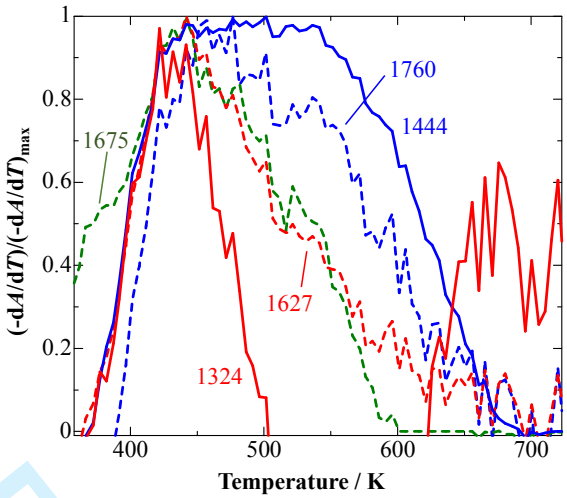


# Figure 5

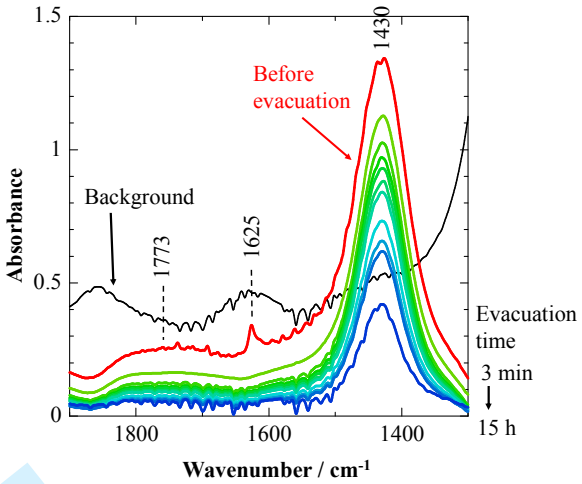


**Figure 6**

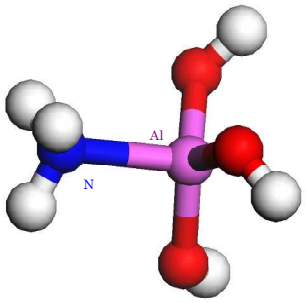


**Figure 7**

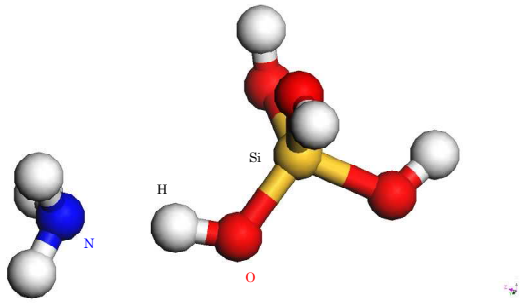


# Figure 8

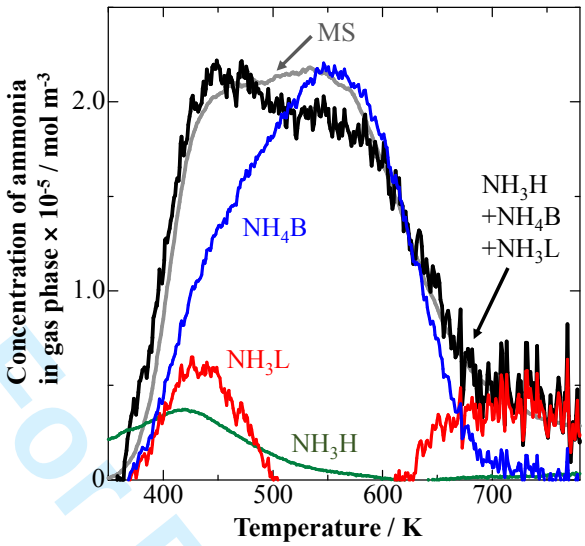


# Figure 9

**Graphical abstract**

**Assignments of Bending Vibrations of Ammonia Adsorbed on Solid Surfaces**

S. Suganuma*, Y. Murakami, J. Ohyama, T. Torikai, K. Okumura, and N. Katada

Bending vibration bands in infrared (IR) spectra of ammonia adsorbed on Brønsted and Lewis acid sites, and hydrogen-bonded species were assigned with an aid of density functional theory.

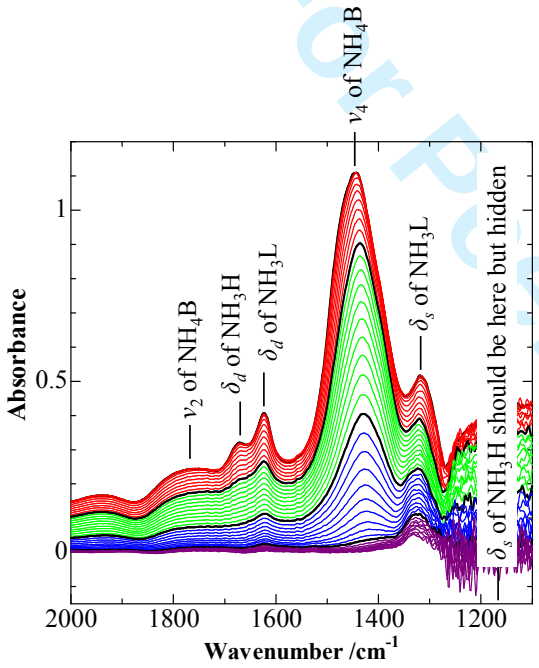

Table 1 Employed oxide samples

| Description | Origin |
|---|---|
| $Al_2O_3$ | Reference catalyst JRC-ALO6 supplied by Reference Catalyst Division, Catalysis Society of Japan, as received |
| $ZrO_2$ | Hydrolysis of $Zr(ONO_3)_2$ with $NH_4OH$ in an aqueous solution followed by calcination at 773 K for 4 h |
| $TiO_2$ | Hydrolysis of $Ti[OCH(CH_3)_2]$ with $H_2O$ in ethanol followed by calcination at 773 K for 4 h [8] |
| USY | Small particles (diameter < 50 nm) of USY prepared from a commercial sample of NaY zeolite (HSZ-320NAA from Tosoh, $SiO_2/Al_2O_3$ = 5.5) by ion-exchange with $NH_4NO_3$, steaming at 823 K with $H_2O$ (18 mol%) / $N_2$ and treatment with $NH_4NO_3$ at 353 K [9] |
| MOR | Ion-exchange of JRC-Z-M15 with $Si/Al_2$ = 15 (Reference catalyst, Reference Catalyst Division, Catalysis Society of Japan) with $NH_4NO_3$ at 353 K. |

Table 2 Calculated and observed wavenumbers. All the calculations have been corrected by multiplying with 0.9630, because the OH stretching wavenumber was calculated to be 3798 $cm^{-1}$ under the same conditions while it was observed at 3657 $cm^{-1}$.

| Entry | Description | Wavenumber ($cm^{-1}$) of $\delta_s$ ($NH_3$) or $\nu_4$ ($NH_4$) | | $\delta_d$ ($NH_3$) or $\nu_2$ ($NH_4$) | |
|---|---|---|---|---|---|
| | | calc. | obs. | calc. | obs. |
| 1 | $H_3N{\rightarrow}Al(OH)_3$ | 1206 | 1224[a] | 1602, 1617 | 1624[a] |
| | $H_3N/Al_2O_3$ | 1226 | 1224 | 1593, 1606 | 1624 |
| 2 | $H_3N{\rightarrow}Zr(OH)_4$ | 1134 | 1173[b] | 1566, 1602 | 1602[b] |
| 3 | $H_3N{\rightarrow}Ti(OH)_4$ | 1154 | 1168[c] | 1592, 1630 | 1599[c] |
| | $H_3N/TiO_2$ | 1156 | 1168 | 1613, 1653 | 1599 |
| 4 | $H_3N{\cdots}H\text{-}O\text{-}Si(OH)_3$ | 1123 | | 1601, 1615 | |
| 5 | Free $NH_3$ | 1050 | 1084 | 1607, 1634 | 1627 |
| 6 | $NH_4{\cdots}FAU$ | 1319, 1436, 1495 | 1450[d] | 1640, 1675 | 1674, 1774 |
| 7 | $NH_4{\cdots}BEA$ | 1344, 1472, 1511 | 1450[d] | 1673, 1686 | 1698 |
| 8 | $NH_4{\cdots}MFI$ | 1345, 1473, 1500 | 1450[d] | 1675, 1676 | |
| 9 | $NH_4{\cdots}MOR$ | | 1450[d] | | 1582, 1804 |
| 10 | Free $NH_4^+$ | 1430, 1444, 1473 | | 1681, 1694 | |

a: Observed on $Al_2O_3$. b: Observed on $ZrO_2$. c: Observed on $TiO_2$. d: It looks that a broad band was formed from peaks at 1395, 1445 and 1490 $cm^{-1}$.

Table 3 Final coordinates of entry 1, $H_3N \rightarrow Al(OH)_3$ (Å)

| ID | ATOM | X | Y | Z |
|---|---|---|---|---|
| 1 | N | -4.081580 | 0.773485 | -0.684991 |
| 2 | Al | -2.421710 | -0.000899 | 0.261624 |
| 3 | O | -1.463078 | 1.461537 | 0.385450 |
| 4 | O | -1.945003 | -1.183342 | -0.940260 |
| 5 | O | -3.209663 | -0.585120 | 1.715469 |
| 6 | H | -3.895919 | 1.721776 | -1.025207 |
| 7 | H | -4.871509 | 0.813296 | -0.033480 |
| 8 | H | -4.352062 | 0.192178 | -1.483844 |
| 9 | H | -3.068668 | -1.504843 | 1.985993 |
| 10 | H | -1.036146 | -1.165325 | -1.275970 |
| 11 | H | -1.152732 | 1.738705 | 1.260736 |

Table 4 Final coordinates of entry 2, $H_3N \rightarrow Zr(OH)_4$ (Å)

| ID | ATOM | X | Y | Z |
|---|---|---|---|---|
| 1 | N | -4.168566 | 0.747810 | -1.088112 |
| 2 | Zr | -2.223629 | 0.445466 | 0.507362 |
| 3 | O | -1.337929 | 0.855829 | -1.268799 |
| 4 | O | -2.900826 | -1.442372 | 0.656379 |
| 5 | H | -3.997108 | 1.611308 | -1.610041 |
| 6 | H | -5.080284 | 0.836977 | -0.633345 |
| 7 | H | -4.219785 | -0.011671 | -1.771089 |
| 8 | H | -3.409282 | -1.952950 | 1.302386 |
| 9 | H | -0.375092 | 0.954185 | -1.350894 |
| 10 | O | -0.632334 | 0.427492 | 1.721550 |
| 11 | O | -3.288680 | 1.931244 | 1.395828 |
| 12 | H | -2.968697 | 2.375267 | 2.199095 |
| 13 | H | -0.117290 | -0.222984 | 2.217786 |

Table 5 Final coordinates of entry 3, $H_3N \rightarrow Ti(OH)_4$ (Å)

| ID | ATOM | X | Y | Z |
|---|---|---|---|---|
| 1 | N | -4.092437 | 0.693477 | -1.075752 |
| 2 | Ti | -2.278168 | 0.467780 | 0.460448 |
| 3 | O | -1.374531 | 0.803940 | -1.160820 |
| 4 | O | -2.836046 | -1.306636 | 0.670554 |
| 5 | H | -4.293349 | 1.691254 | -1.178703 |
| 6 | H | -4.956200 | 0.223519 | -0.796682 |
| 7 | H | -3.804529 | 0.330606 | -1.987766 |
| 8 | H | -3.312982 | -1.616478 | 1.459563 |
| 9 | H | -0.413361 | 0.939213 | -1.078482 |
| 10 | O | -0.836793 | 0.534933 | 1.653737 |
| 11 | O | -3.256497 | 1.859914 | 1.266797 |
| 12 | H | -2.848851 | 2.216879 | 2.077195 |
| 13 | H | -0.415759 | -0.282800 | 1.968012 |

Table 6 Final coordinates of entry 4: $H_3N \cdots H_a$-O-$Si(OH)_3$ (Å)

| ID | ATOM | X | Y | Z |
|---|---|---|---|---|
| 1 | N | -3.149728 | 1.931289 | 3.646233 |
| 2 | Si | -2.145739 | -0.054356 | 0.422084 |
| 3 | O | -0.687346 | 0.748297 | 0.516893 |
| 4 | O | -2.609491 | -0.289966 | -1.153493 |
| 5 | O | -1.808672 | -1.499749 | 1.203879 |
| 6 | H | -2.478569 | 2.703158 | 3.620246 |
| 7 | H | -4.046269 | 2.324543 | 3.943574 |
| 8 | H | -2.843868 | 1.294843 | 4.386341 |
| 9 | H | -2.555336 | -2.118869 | 1.261648 |
| 10 | H | -1.916167 | -0.649890 | -1.730019 |
| 11 | H | 0.013948 | 0.231239 | 0.947003 |
| 12 | O | -3.394994 | 0.777003 | 1.062552 |
| 13 | H | -3.281645 | 1.152197 | 1.982249 |

Table 7 Final coordinates of entry 5, free $NH_3$ (Å)

| ID | ATOM | X | Y | Z |
|---|---|---|---|---|
| 1 | N | -0.010477 | -0.014395 | 0.024595 |
| 2 | H | -0.316066 | -0.446786 | -0.852060 |
| 3 | H | -0.315673 | 0.961076 | -0.039395 |
| 4 | H | 1.010932 | 0.022475 | -0.039001 |

Table 8 Final coordinates of entry 6, free $NH_4^+$ (Å)

| ID | ATOM | X | Y | Z |
|---|---|---|---|---|
| 1 | N | -0.034779 | -0.005575 | 0.000586 |
| 2 | H | -0.313716 | -0.461686 | -0.881707 |
| 3 | H | -0.324085 | 0.984404 | -0.017597 |
| 4 | H | 0.989452 | -0.062860 | 0.108671 |
| 5 | H | -0.491362 | -0.481867 | 0.793339 |